

Open-Vocabulary Camouflaged Object Segmentation

Youwei Pang^{1,2}, Xiaoqi Zhao^{1,2}, Jiaming Zuo², Lihe Zhang¹ and Huchuan Lu^{1,3}

¹Dalian University of Technology ²X3000 Inspection Co., Ltd ³Peng Cheng Laboratory

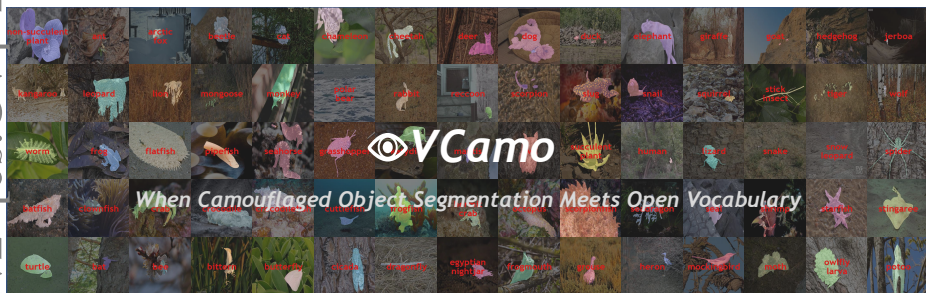


Fig. 1: A new large-scale dataset **OVCamo** for the proposed new challenging task, open-vocabulary camouflaged object segmentation.

Abstract. Recently, the emergence of the large-scale vision-language model (VLM), such as CLIP, has opened the way towards open-world object perception. Many works have explored the utilization of pre-trained VLM for the challenging open-vocabulary dense prediction task that requires perceiving diverse objects with novel classes at inference time. Existing methods construct experiments based on the public datasets of related tasks, which are not tailored for open vocabulary and rarely involve imperceptible objects camouflaged in complex scenes due to data collection bias and annotation costs. To fill in the gaps, we introduce a new task, open-vocabulary camouflaged object segmentation (OVCOS), and construct a large-scale complex scene dataset (**OVCamo**) containing 11,483 hand-selected images with fine annotations and corresponding object classes. Further, we build a strong single-stage open-vocabulary camouflaged object segmentation transformer baseline **OVCoser** attached to the parameter-fixed CLIP with iterative semantic guidance and structure enhancement. By integrating the guidance of class semantic knowledge and the supplement of visual structure cues from the edge and depth information, the proposed method can efficiently capture camouflaged objects. Moreover, this effective framework also surpasses previous state-of-the-arts of open-vocabulary semantic image segmentation by a large margin on our OVCamo dataset. With the proposed dataset and baseline, we hope that this new task with more practical value can further expand the research on open-vocabulary dense prediction tasks. The code and data will be available in the future.

Keywords: Open Vocabulary · Camouflaged Object Segmentation

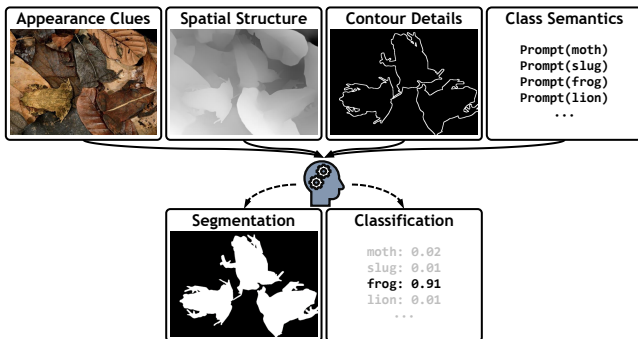


Fig. 2: The perception and recognition of camouflaged objects require the collaboration of information from multiple sources such as appearance clues, spatial structure, contour details, and object semantics.

1 Introduction

The ability to identify and reason about object regions in a visual scene is essential for a wide range of human activities. As a complex and fundamental task in computer vision, detecting and segmenting objects with diverse appearances in complex scenes is also an important challenge, which is crucial for applications across vision and robotics fields, including autonomous driving [3], medical image analysis [28], and intelligent robotics [62], to name a few. In the past few years, numerous typical methods [6, 7, 19, 54] have emerged with the help of a mass of labeled data, which have greatly promoted the development of related fields such as semantic image segmentation (SIS) [11, 44]. However, existing works have mainly focused on predefined closed-set scenarios, where all semantic concepts are seen during both the inference and training phases. Such a scenario setting oversimplifies the real-world complexity. To this end, many explorations have been contributed to open vocabulary settings [61].

Recently, large-scale pre-trained visual language models (VLMs) such as CLIP [9, 37] have been gaining attention. Image-text matching-based learning mechanism provides them with the ability to align textual and visual signals well, and many works demonstrate their potential for open vocabulary tasks. Besides, data plays an important role in open-vocabulary tasks. Existing open-vocabulary semantic image segmentation (OVSIS) tasks rely on related public datasets [4, 12, 34, 35, 57], while they are not designed for the open-vocabulary setting, and there is high semantic similarity between their class definitions as revealed in [48]. Due to the data collection bias and annotation cost constraints, the existing open-vocabulary benchmarks lack special attention to finely perceive the objects of interest in concealed scenes. And the widely used VLMs are pre-trained on image-text pairs with inherent object concept bias, thus, their ability to segment objects in complex scenes remains to be verified.

In this paper, we introduce a new open-vocabulary segmentation task OVCOS dedicated to analyzing camouflaged object perception in diverse natural

scenes. And a large-scale data benchmark, named OVCamo, is carefully constructed. Besides, we also design a strong baseline OVCoser for the proposed OVCOS, based on the VLM-driven single-stage paradigm. The camouflage¹ arises from several sources, including similar patterns to the environment (*e.g.*, color and texture) and imperceptible attributes (*e.g.*, small size and heavy occlusion) as statistically illustrated in Fig. 4. Considering the imperceptible appearance of camouflaged objects, accurate recognition and capture actually depend more on the cooperation of multi-source knowledge. As shown in Fig. 2, in addition to visual appearance cues, we introduce the depth for the spatial structure of the scene, the edge for the regional changes about objects, and the text for the context-aware class semantics. Considering the cooperative relationship between class recognition and object perception, the iterative learning strategy is introduced to feed back the optimized semantic relationship, resulting in more accurate object semantic guidance. This top-down conceptual reinforcement can further optimize open-vocabulary segmentation performance. With the help of the iterative multi-source information joint learning strategy, our method OVCoser shows good performance in the proposed OVCOS task.

In summary, our contributions are three-fold as follows:

- **New Challenge.** In view of the limitations of the existing OVSIS, we introduce a more challenging OVCOS task for open-vocabulary segmentation of camouflaged objects.
- **New Benchmark.** A new large-scale benchmark OVCamo with diverse samples carefully collected from existing publicly available data is proposed to better evaluate and analyze the generalization of algorithms on the proposed task.
- **Strong Baseline.** We build a robust single-stage baseline based on CLIP, in which the proposed iterative semantic guidance and structure enhancement are embedded. Under the joint optimization of multi-source information, our approach OVCoser outperforms existing OVSIS algorithms on the new benchmark.

2 Related Works

Vision-Language Pre-training. The core goal of visual-language pre-training is to learn generic representations of vision and language, and connect visual and language concepts. Early approaches [5, 25, 26, 42] are based on some relatively small and clean public datasets, which limits their achievable performance, and their fine-tuning on specific downstream tasks hinders application flexibility. In [33], image-text pairs collected from the Internet bring clear performance improvement for the retrieval task. This also indirectly encourages subsequent further exploration, such as CLIP [9, 37]. It benefits from the larger scale of noisy data from web pages covering diverse and rich concepts and exhibits impressive

¹ To ensure the reliability of the definition, we follow existing published literature and collect data from the camouflage perception field, *i.e.*, CSU [15].

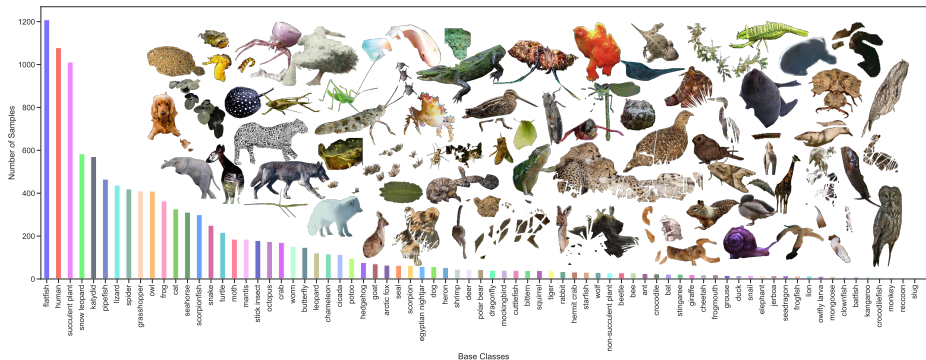


Fig. 3: Class distribution in the proposed OVCamo dataset and some visual examples.

open-vocabulary capabilities. This work introduces CLIP as the bedrock of open-vocabulary capability and borrows its strong image-text matching capability to build an effective baseline for the OVCOS task.

Open Vocabulary Semantic Image Segmentation (OVSIS). Although a variety of pipelines have emerged as summarized in [61], from an overall perspective, their efforts are similar, namely, *how to align class name/description semantic embedding with visual features to anchor relevant object cues in the representation space*. The early pioneer work [55] attempts to connect word concepts and semantic relations, and encodes word concept hierarchy to parse images. Due to the leading performance of the VLM on the image-text joint modeling, it has been gradually applied in the OVSIS field. In terms of structure, existing schemes can be roughly categorized into two types: two-stage [27, 47, 49, 53] and single-stage [10, 52, 58]. In [53], a rough segmentation map for each class is created from a VLM and then refined by the test-time augmentation. These rough maps are utilized as pseudo-labels for subsequent fine segmentation by stochastic pixel sampling. SimSeg [49] adopts a cascaded design including class-agnostic proposal generation by MaskFormer [7] and class assignment by CLIP [37]. Furthermore, OVSeg [27] fine-tunes CLIP on the noisy but diverse data to improve its generalization to masked images. In lieu of using existing SIS models, a text-to-image diffusion model is introduced to generate mask features with implicit image captions in [47].

The single-stage design is more flexible and simpler. MaskCLIP [58] directly modifies CLIP for semantic segmentation without training, while SAN [48] achieves better performance with the help of adapters. CAT-Seg [10] highlights the importance of the cost aggregation between image and text embeddings for the OVSIS decoding. Recent FC-CLIP [52] investigates the hierarchical CLIP image encoder. Although these methods show impressive OVSIS performance, they still follow the generalized segmentation paradigm [6, 7] in SIS, ignoring valuable auxiliary cues for object perception. This also causes them to struggle with objects camouflaged in complex scenes. Unlike them, our method, which is tailored for OVCOS, can effectively tap into the camouflaged object by in-

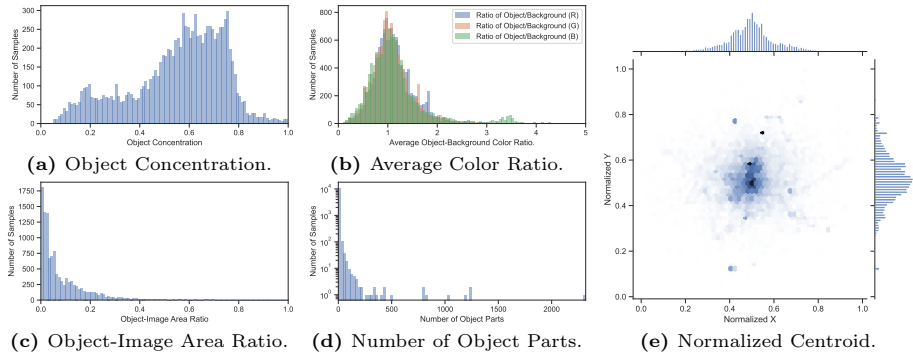


Fig. 4: Attribute visualization of objects in the proposed OVCamo dataset, including object concentration, object-background color ratio, object-image area ratio, number of object parts, and normalized centroid. Please refer to Tab. 1 for more details about attributes.

tegrating task-specific multi-source knowledge from visual appearance, spatial structure, object contour, and class semantics.

Camouflaged Scene Understanding (CSU). This is a research hotspot in the computer vision community, aiming to perceive objects with camouflage [15]. Different from traditional object detection, CSU is obviously a more challenging problem. It can be applied in some specific fields, such as medical analysis [13,16] and agricultural management [29,39]. This topic is currently defined as the class-agnostic form, focusing on the area of camouflaged objects in the visual scene. The available work [8, 13, 14, 21, 24, 36, 51] to date has demonstrated promising performance on existing data benchmarks [2, 8, 14, 23, 32, 41]. Unlike previous settings, the proposed OVCOS task requires further perception of object classes. Admittedly, the publicly available data provides critical support for this new task. It helps us take the first step.

3 OVCamo Dataset

This work focuses on open-vocabulary segmentation in the camouflaged scene. It enriches the connotation of OVSIS and provides a more challenging benchmark.

Image Collection. Our data is collected from existing CSU datasets that have finely annotated segmentation maps. Specifically, the OVCamo integrates 11,483 hand-selected images covering 75 object classes reconstructed from several public datasets [2, 8, 14, 50, 56]. The distribution of the number of samples in different classes is shown in Fig. 3. Meanwhile, we consider attributes of objects when selecting images, such as object concentration, average color ratio, object-image area ratio, number of object parts, and normalized centroid. Tab. 1 gives their definitions. And Fig. 4 visualizes the attribute distribution of the proposed dataset. The camouflaged objects of interest usually have complex shape Fig. 4a, high similarity to the background Fig. 4b, and small size Fig. 4c. And the image

Table 1: Attributes involved in the dataset analysis.

Attribute	Description
Object Concentration	Object pixel concentration, which calculates the area ratio between the object region and its minimum rotatable bounding box.
Average Color Ratio	Color ratio of the object to the background, which calculates the average of the three color channels in their respective regions.
Object-Image Area Ratio	Area ratio of the object relative to the image.
Number of Object Parts	Number of separate areas in the image that belong to the object.
Normalized Centroid	Object centroid coordinates, which are normalized using the image shape.

often contains multiple camouflaged objects or sub-regions with a central bias as shown in Fig. 4d and Fig. 4e.

Re-annotation. The original annotation cannot be used directly in the open-vocabulary setting, due to the following semantic ambiguities caused by different annotation standards, *i.e.*, 1) Broad concepts, such as “fish” and “bug”; 2) Vague definitions, such as “small fish” and “black cat”; 3) Inconsistent granularity, such as the coexistence of “orchid mantis” and “mantis”; 4) Non-entity concepts, such as “other”. These issues can lead to unreasonable and unreliable results for the open-vocabulary prediction as discussed in [59]. To this end, we re-label the classes of all camouflaged objects and take the generality of the concept as the criterion for class definition, which also ensures lower semantic similarity.

Data Division. To objectively evaluate the open-vocabulary segmentation algorithm on unseen classes, we assign as many classes as possible to the test set and control the sample ratio of the training set to the testing set to be 7:3. Specifically, 14 classes in the dataset are taken as the training set and all the remaining 61 classes are used for testing. Such a setting follows the existing practice in OVSIS where the number of seen classes (*e.g.*, 171 [4]) is usually fewer than unseen classes (*e.g.*, 847 [57]) which is also closer to the real-world setting. Such a setup can ensure the quantity of training samples while reinforcing the complexity of the test set. Finally, the overall ratio of samples is 7713:3770.

4 Methodology

In this section, we introduce a strong baseline OVCoser. The overall framework is first described, followed by the details of the key components.

4.1 Overall Architecture

We follow the common encoder-decoder paradigm and the pipeline is shown in Fig. 5. Specifically, we first leverage the textual encoder \mathbf{E}_t of the frozen CLIP to extract semantic embedding f_t from the class label set \mathcal{C} , and the visual encoder \mathbf{E}_v to extract multi-scale image features $\{f^i\}_{i=1}^5$. Both of them are fed into the decoder as the information bedrock of object segmentation, as shown in Fig. 6. Structural cues such as depth and edge are also introduced to

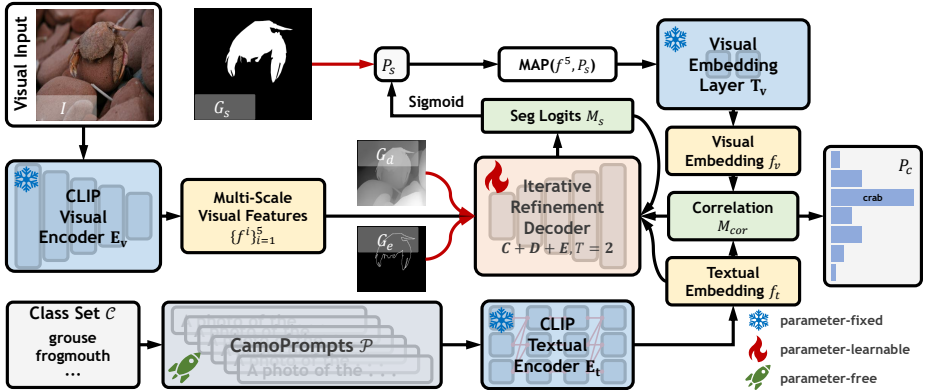


Fig. 5: Overview of our single-stage open-vocabulary camouflaged object segmentation framework, OVCosNet. It is based on the frozen CLIP model which includes feature encoder E_v and embedding layer T_v for visual appearance cues and textual encoder E_t for class semantic information. The well-constructed prompt template set CamoPrompts \mathcal{P} enables textual embedding f_t to be more appropriate to OVCOS. In the iterative refinement decoder (Fig. 6), a more accurate class-related segmentation P_s , can be obtained with the assistance of the semantic guidance \mathcal{C} (Fig. 7a) from the class semantic and the structure enhancement (Fig. 7b) from the auxiliary depth and edge supervisions, *i.e.*, D and E . After being masked average pooled (MAP) by P_s , the high-level feature f^5 is used to assign a class P_c to the object from the class set \mathcal{C} .

assist the iterative refinement process. Finally, the class-related segmentation P_s which is the segmentation logits M_s after the **sigmoid** function processing, is used to remove the interference from the background in the high-level image feature and guide the generation of object-oriented visual representation f_v . And the class label P_c is determined by the similarity matching between f_v and f_t .

Details of E_v and T_v . In the proposed model, the visual encoder E_v and embedding layer T_v together are used to extract the high-level embedding corresponding to the object of interest in the input image. The two independent sub-networks are split from the visual network of CLIP [9, 37]. E_v contains all the feature encoding layers for extracting the multi-scale image features. And T_v corresponds to the final high-dimensional projection layer, which is used to convert the high-level image feature f^5 into the visual embedding vector f_v .

4.2 Semantic Guidance (SG)

The class label definition usually is independent of the image scene. It is very important to fully utilize the class prior for object recognition in complex scenes. In the proposed decoder, normalized textual embedding is introduced into each stage to highlight semantically relevant cues. As shown in Fig. 7a, we design a semantic guidance component SG to inject concept cues into the self-enhancement of the image feature.

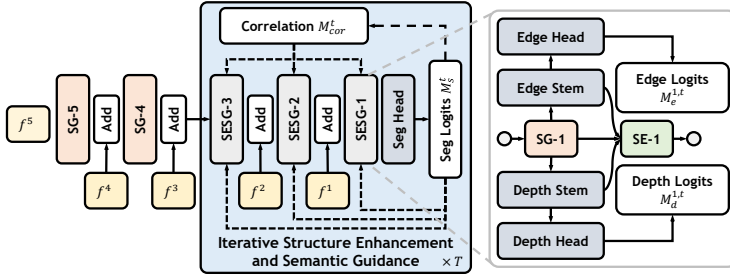


Fig. 6: Proposed pipeline of the iterative refinement decoder with semantic guidance (SG) and structure enhancement (SE) components denoted as “SG- \star ” and “SE- \star ”. t and T denote the current step and total number of iterations, respectively.

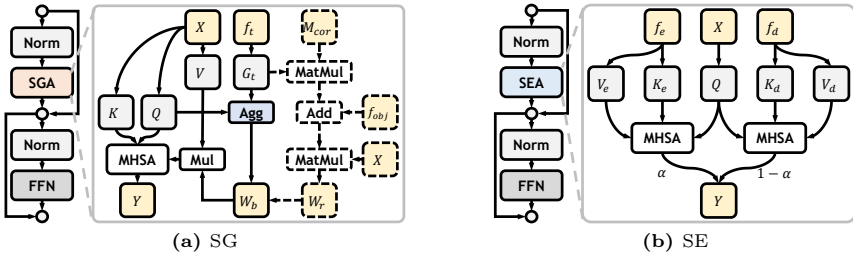


Fig. 7: Proposed semantic guidance (SG) and structure enhancement (SE) components in which semantic guidance attention (SGA) and structure enhancement attention (SEA) are embedded. The dashed blocks represent the feedback paths that come into play during iteration.

Semantic Guidance Attention (SGA). Specifically, the normalized image feature X is linearly mapped to Q , K , and V , while the textual embedding f_t is transformed to the class guidance vector G_t . The similarity between Q and G_t reflects the activation of different classes in spatial locations. In **Agg** of Fig. 7a, the base weight W_b for the spatial guidance is obtained after highlighting the most relevant class information by **softmax** operation. And then V is modulated and fed into MHSA, *i.e.*, multi-head self-attention [45].

4.3 Structure Enhancement (SE)

Existing methods demonstrate that low-level structural information, such as the edge [43] and the depth [46], plays an important role in CSU, which is closely related to the mechanism of the human visual system. So the SE component attached to the low-level SG is proposed to integrate the edge-aware and depth-aware cues and improve the structural details. Specifically, the output of the SG is fed into two separate branches containing the convolutional stem and head for the edge and depth estimation as shown in Fig. 6. The edge and depth logits maps, *i.e.*, M_e^i and M_d^i , from the head in the branch of the layer $i \in \{1, 2, 3\}$

are directly supervised. And the outputs f_e^i and f_d^i of the stem are fed into the SE. In the **structure enhancement attention (SEA)**, they independently update the normalized visual features X using MHSA [45], and the corresponding outputs are combined with the learnable weight α as in Fig. 7b.

4.4 Iterative Refinement

In the SG component, the aggregation process between image features and class semantics is not aligned and requires data-driven optimization. Considering the aligned embedding space of the pre-trained CLIP, we introduce the correlation matrix M_{cor} between the visual and textual embeddings into the SG as shown in Fig. 7a. Meanwhile, due to the emphasis of the decoder output on the object region, the object-aware representation f_{obj} is also inputted, which comes from the image features pooled by the coarse segmentation prediction in the last iteration. By combining the two, we obtain task-oriented object cues, which is actually inspired by the top-down attention mechanism in the human cognitive system [1, 22]. The spatial activation map W_r of such object cues over image features is used to re-modulate W_b . Besides, the SE in the iteration also helps the model to further optimize the texture details. To benefit as much as possible from the assistance from structure enhancement while avoiding over-computation, we set the iteration entry to the third decoding layer as shown in Fig. 6.

4.5 CamoPrompts

As mentioned in [37], prompt engineering and ensembling are important for the transfer performance of CLIP on downstream tasks, and the prompt template should be more relevant to the data type. Because additional task-related cues are generally able to impose the necessary contextual constraint to the flexible CLIP. Hence, instead of common practices [18, 37, 60], we design a simpler yet more effective template set CamoPrompts tailored for OVCOS to decorate the class name, and average their textual embeddings as the final semantic embedding for each class. Its full form is depicted in Tab. 4, while it also achieves better classification performance in comparison with other forms.

4.6 Supervision

In each iteration, in addition to semantic object segmentation, we also need to perform depth estimation and edge estimation as auxiliary tasks. For the segmentation prediction, we follow the commonly used weighted segmentation loss function $l_s^t = l_s(P_s^t, G_s)$ [43, 51]. For the edge estimation, considering the imbalance problem of positive and negative samples, we introduce the dice loss function as $l_e^{i,t} = l_e(P_e^{i,t}, G_e)$. The summation of L1 and SSIM losses, *i.e.*, $l_d^{i,t} = l_d(P_d^{i,t}, G_d)$, is used for the depth estimation. The total loss L of our method can be formulated as follows:

$$L = \sum_{t=1}^T \left[l_s^t + \sum_{i=1}^3 \left(l_e^{i,t} + l_d^{i,t} \right) \right], \quad (1)$$

Table 2: Comparison with recent state-of-the-art CLIP-based open-vocabulary semantic image segmentation methods with different training settings on the proposed OVCamo dataset. The best three results are highlighted in **red**, **green** and **blue**.

Model	VLM	Feature Backbone	Text Prompt	cS _m ↑	cF _β ^{sw} ↑	cMAE ↓	cF _β ↑	cE _m ↑	cIoU ↑
<i>Test on OVCamo with the weight trained on COCO.</i>									
SimSeg ²¹ [49]	CLIP-ViT-B/16 [37]	ResNet-101 [20]	Learnable [60]	0.128	0.105	0.838	0.112	0.143	0.094
OVSeg ²² [27]	CLIP-ViT-L/14 [37]	Swin-B [30]	[18]	0.341	0.306	0.584	0.325	0.384	0.273
ODISE ²³ [47]	CLIP-ViT-L/14 [37]	StableDiffusionv1.3 [40]	[17]	0.409	0.339	0.500	0.341	0.421	0.302
SAN ²³ [48]	CLIP-ViT-L/14 [37]	ViT Adapter [18]	[18]	0.414	0.343	0.489	0.357	0.456	0.319
CAT-Seg ²³ [10]	CLIP-ViT-L/14 [37]	Swin-B [30]	[37]	0.430	0.344	0.448	0.366	0.459	0.310
FC-CLIP ²³ [52]	CLIP-ConvNeXt-L [9]	—	[18]	0.374	0.306	0.539	0.320	0.409	0.285
<i>Finetune on OVCamo with the weight trained on COCO.</i>									
SimSeg ²¹ [49]	CLIP-ViT-B/16 [37]	ResNet-101 [20]	Learnable [60]	0.098	0.071	0.852	0.081	0.128	0.066
OVSeg ²² [27]	CLIP-ViT-L/14 [37]	Swin-B [30]	[18]	0.164	0.131	0.763	0.147	0.208	0.123
ODISE ²³ [47]	CLIP-ViT-L/14 [37]	StableDiffusionv1.3 [40]	[17]	0.182	0.125	0.691	0.219	0.309	0.189
SAN ²³ [48]	CLIP-ViT-L/14 [37]	ViT Adapter [18]	[18]	0.321	0.216	0.550	0.236	0.331	0.204
CAT-Seg ²³ [10]	CLIP-ViT-L/14 [37]	Swin-B [30]	[37]	0.185	0.094	0.702	0.110	0.185	0.088
FC-CLIP ²³ [52]	CLIP-ConvNeXt-L [9]	—	[18]	0.124	0.074	0.798	0.088	0.162	0.072
<i>Train on OVCamo.</i>									
SimSeg ²¹ [49]	CLIP-ViT-B/16 [37]	ResNet-101 [20]	Learnable [60]	0.053	0.049	0.921	0.056	0.098	0.047
OVSeg ²² [27]	CLIP-ViT-L/14 [37]	Swin-B [30]	[18]	0.024	0.046	0.954	0.056	0.130	0.046
ODISE ²³ [47]	CLIP-ViT-L/14 [37]	StableDiffusionv1.3 [40]	[17]	0.187	0.119	0.700	0.211	0.298	0.167
SAN ²³ [48]	CLIP-ViT-L/14 [37]	ViT Adapter [18]	[18]	0.275	0.202	0.612	0.220	0.318	0.189
CAT-Seg ²³ [10]	CLIP-ViT-L/14 [37]	Swin-B [30]	[37]	0.181	0.106	0.719	0.123	0.196	0.094
FC-CLIP ²³ [52]	CLIP-ConvNeXt-L [9]	—	[18]	0.080	0.076	0.872	0.090	0.191	0.072
Ours	CLIP-ConvNeXt-L [9]	—	CamoPrompts	0.579	0.490	0.337	0.520	0.615	0.443

where t and i are used to index iterations and layers, respectively. And the total number T of iterations is set to 2 as mentioned in Sec. 5.3.

5 Experiments

5.1 Implementation Details

Dataset Settings. As mentioned in Sec. 3, the proposed dataset is divided according to classes into two disjoint subsets, *i.e.*, \mathcal{C}_{seen} and \mathcal{C}_{unseen} . The former contains 14 classes for training and the latter contains the remaining 61 classes for testing. The proposed dataset itself is provided with only images and masks. We use the typical monocular depth estimation method DPT [38] to obtain the depth map G_d for training, while the edge map G_e is generated by dilating and eroding operations. To avoid information leakage during testing, we use depth and edge maps only in the training phase. And these generated depth maps and edge maps will be made publicly available with the dataset.

Model Settings. Following previous settings in [48, 49, 52], the pre-trained CLIP is frozen during training, and the remaining parameters are learnable and are randomly initialized. The AdamW [31] optimizer with the learning rate of 3e-6, weight decay of 5e-4, batch size of 4, and training epoch of 30 is used to optimize model parameters. Some basic data augmentations including random flipping, rotating, and color jittering, are introduced to preprocess training data. The input data is bilinearly interpolated to 384×384 during training and inference.

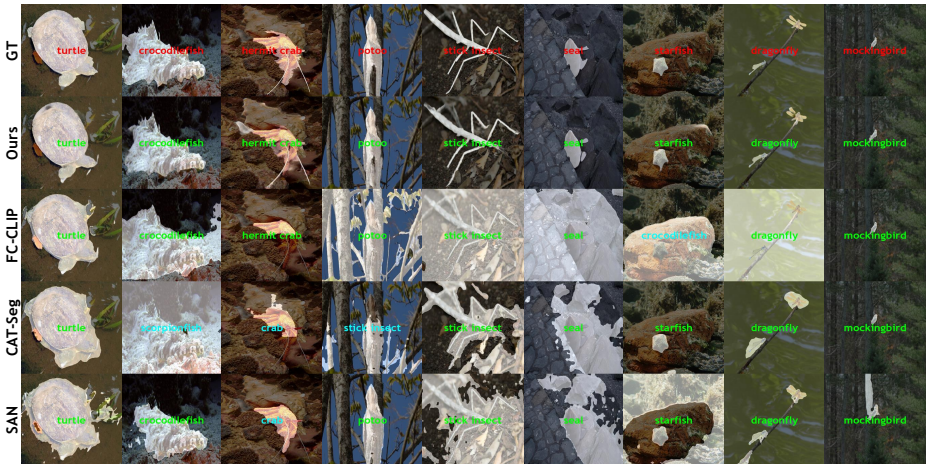


Fig. 8: Visual results on OVCamo. Existing methods are either disrupted by chaotic backgrounds, imperceptible appearances, blurry details, or severe occlusion, while our algorithm can effectively capture and remain well-exposed object details. And three different colors are used to represent **human annotations**, **correct predictions**, and **incorrect predictions**.

Evaluation Protocol. To reasonably evaluate the performance of OVCOS, we modify the metrics in the original CSU task [8, 13] to cS_m , cF_β^ω , $cMAE$, cF_β , cE_m , and $cIoU$ which follows the common settings in the OVSIS field [10, 27, 48, 49, 52, 61] and takes into account both classification and segmentation.

5.2 System-level Comparison

To show the complexity of the proposed OVCOS task and also to verify the effectiveness of the proposed method, we compare OVCoser with several recent state-of-the-art methods in OVSIS, including [10, 27, 47–49, 52]. Since this is a new task, existing methods need to be re-evaluated to understand their generalization ability. Based on the public code and weights trained on COCO-Stuff [4] provided by the authors, we show the performance of these methods under three different testing schemes, including S.I) testing directly with their trained weights; S.II) further fine-tuning based on trained weights before testing; and S.III) testing after re-training directly on our training set.

Quantitative Evaluation. For the sake of fairness in comparisons, we report the performance of the “Large” versions for these methods, except for SimSeg [49] where the authors only provide the “Base” version. All results are summarized in Tab. 2 and our approach consistently outperforms these competitors. It is worth noting that existing methods perform better at S.I. This may be attributed to the training process on the larger-scale COCO-Stuff dataset, which provides a more general understanding of the concepts. However, direct fine-tuning (*i.e.*, S.II) may destroy this knowledge and even cause oblivion to some extent, result-

Table 3: Ablation comparison of proposed components. Δ represents the *average relative gain* in performance of the corresponding model over the baseline for OVCOS. \mathcal{P} : CamoPrompts. \mathcal{C} : Semantic guidance. \mathcal{D} : Depth estimation auxiliary task. \mathcal{E} : Edge estimation auxiliary task. T : Number of iterations which is set to 2 by default due to the best performance. “ $\limsup_{P_s \rightarrow G_s}$ Perf.”: The ideal performance for our framework.

Model	cS _m ↑	cF _β ^w ↑	cMAE ↓	cF _β ↑	cE _m ↑	cIoU ↑	Δ
<i>Comparison of the proposed modules.</i>							
Baseline	0.517	0.408	0.374	0.451	0.549	0.359	0.0%
+ \mathcal{P}	0.543	0.435	0.346	0.480	0.581	0.383	6.3%
+ \mathcal{P}, \mathcal{C}	0.550	0.453	0.341	0.491	0.597	0.397	9.1%
+ $\mathcal{P}, \mathcal{C}, \mathcal{D}$	0.565	0.473	0.336	0.507	0.606	0.422	12.6%
+ $\mathcal{P}, \mathcal{C}, \mathcal{E}$	0.567	0.481	0.339	0.511	0.607	0.432	13.5%
+ $\mathcal{P}, \mathcal{C}, \mathcal{D}, \mathcal{E}$ (i.e., $T = 1$)	0.570	0.488	0.338	0.518	0.610	0.436	14.5%
<i>Comparison of the proposed iterative refinement.</i>							
$T = 1$	0.570	0.488	0.338	0.518	0.610	0.436	14.5%
$T = 2$	0.579	0.490	0.337	0.520	0.615	0.443	15.5%
w/o f_{obj} as in Fig. 7a	0.575	0.487	0.337	0.515	0.611	0.441	14.8%
w/o M_{cor} as in Fig. 7a	0.571	0.476	0.339	0.506	0.608	0.434	13.4%
$T = 3$	0.576	0.484	0.333	0.514	0.614	0.437	14.8%
$\limsup_{P_{seg} \rightarrow G_{seg}}$ Perf.	0.703	0.703	0.297	0.701	0.701	0.701	51.2%

ing in performance degradation. If we follow S.III to re-train them, the relatively small-scale training data may not be enough to train these models with more complex structures. At the same time, the existing methods also lack targeted optimization for the OVCOS task. These problems can lead to further deterioration of performance. However, our approach tailored for OVCOS achieves leading performance by the iterative refinement strategy of multi-source information, which comprehensively considers different characteristics of the task.

Qualitative Evaluation. We also visualize the results of some recent methods on a variety of data in Fig. 8. It can be seen that the proposed method shows better performance and adaptability to diverse objects, including large objects (Col. 1-2), middle objects (Col. 3-5), small objects (Col. 6-9), multiple objects (Col. 8), complex shapes (Col. 3-5), blurred edges (Col. 1-5), severe occlusion (Col. 6), and background interference (Col. 2-6).

5.3 Analysis and Ablation Study

Importance of Modules. To specifically analyze the effect of different components, we evaluate their performance in Tab. 3. As can be seen, the proposed modules all show positive gains. Both the semantic guidance in the class-aware decoding and the structure enhancement from auxiliary tasks of depth and edge estimation consistently boost the final performance. The ablation comparison also demonstrates that explicit guidance of the spatial and contour information is important for the detection of camouflaged objects. Besides, in Tab. 3, we also give the ideal results of our CLIP-driven framework where G_s is treated as P_s .

Table 4: Classification accuracy \mathcal{A} of the plain CLIP using different prompt templates on OVCamo, which is based on the masked average pooling with the ground truth mask.

ID	Prompt Template	\mathcal{A}
0	"<class>" w/o MAP based on ground truth	0.538
<i>Task-generic templates.</i>		
1	"<class>"	0.671
2.1	"The <class>."	0.648
2.2	"the <class>"	0.632
2.3	"A <class>."	0.677
2.4	"a <class>"	0.675
3.1	"A photo of a <class>."	0.684
3.2	"A photo of the <class>."	0.691
3.3	"The photo of a <class>."	0.672
3.4	"The photo of the <class>."	0.680
3.5	"a photo of a <class>"	0.684
3.6	"a photo of the <class>"	0.689
3.7	"the photo of a <class>"	0.675
3.8	"the photo of the <class>"	0.674
4	templates from [37]	0.686
5	templates from [18]	0.682
<i>Task-related templates.</i>		
6.1	"A photo of the camouflaged <class>."	0.681
6.2	"A photo of the concealed <class>."	0.674
6.3	6.1, 6.2	0.685
6.4	"A photo of the <class> camouflaged in the background."	0.684
6.5	"A photo of the <class> concealed in the background."	0.694
6.6	6.4, 6.5	0.694
6.7	"A photo of the <class> camouflaged to blend in with its surroundings."	0.700
6.8	"A photo of the <class> concealed to blend in with its surroundings."	0.697
6.9	6.7, 6.8	0.703
6.10	6.1 - 6.9 i.e., CamoPrompts	0.704

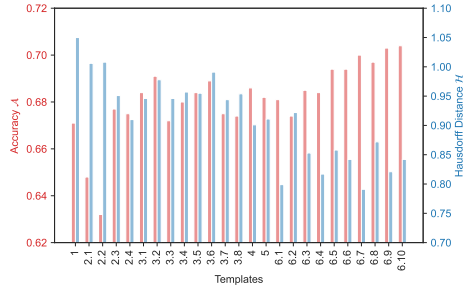


Fig. 9: Illustration of classification accuracy \mathcal{A} and Hausdorff distance \mathcal{H} between the textual embeddings of training and testing class splits by using the plain CLIP on the OVCamo dataset. The approximate negative correlation between them may reveal that the templates that bring training and testing class embeddings closer usually also improve classification accuracy. Tab. 4 shows the details of these templates.

Although our method exhibits leading performance compared to existing methods as shown in Tab. 2, there is still a long way to go to solve this problem. *At the same time, the current ideal performance is still far from the limit, suggesting that future breakthroughs in this field may require more powerful paradigms.*

Importance of Iterative Refinement. The top-down iterative refinement strategy significantly improves the OVCOS performance as shown in Tab. 3. When the number T of iterations is 2, our algorithm obtains the best OVCOS performance. As T increases, there is no further improvement in performance, so it is set to 2 by default. In addition, the correlation guidance M_{cor} from the output space plays an important role, and introducing the object-aware representation f_{obj} also has positive gains.

Importance of CamoPrompts. Our prompt template set CamoPrompts, which takes task attributes into account, shows better performance in Tab. 4. To further understand the influence of different templates on the semantic embedding, we calculate the Hausdorff distance between training and testing class labels in the embedding space, as shown in Fig. 9. The figure presents an interesting phenomenon that those templates with better classification performance tend to reduce the distance, which inspires further explorations for more effective prompt engineering.

Importance Between Edge and Depth. In the proposed SE as shown in Fig. 7b, the interaction components for the edge and depth are combined by a coefficient vector α , which can also reflect the relative importance of the two kinds of information. In Fig. 10, we plot α from different decoding layers. It can be seen

Table 5: Efficiency comparison with other methods. ‘‘Trainable Param.’’ and ‘‘Total Param.’’ stand for the number of trainable and total parameters. In OVSeg [27], the CLIP [37] model is fine-tuned by the authors, resulting in more trainable parameters.

Model	Trainable Param.	Total Param.	FLOPs
SimSeg ²¹ [49]	61M (28.91%)	211M	1.9T
OVSeg ²² [27]	531M (100.00%)	531M	8.0T
ODISE ²³ [47]	28M (1.80%)	1522M	5.5T
SAN ²³ [48]	9M (2.06%)	437M	0.4T
CAT-Seg ²³ [10]	104M (21.22%)	490M	0.3T
FC-CLIP ²³ [52]	20M (5.38%)	372M	0.8T
Ours	7M (1.95%)	359M	0.2T

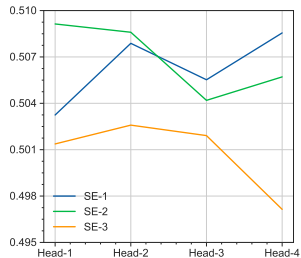


Fig. 10: α corresponding to different heads in Fig. 7b from different decoding layers.

that the values are usually greater than 0.5, which indicates a preference for the edge information flow.

Model Complexity. We compare the proposed method with the CLIP-based competitors [10, 27, 47–49, 52] in terms of the number of trainable and total parameters, and FLOPs. To be fair, we test all methods following the setting of their original inference settings. As can be seen from Tab. 5, our method has fewer trainable parameters ($< 2\%$) and less computational complexity (0.2T), which is superior to these competitors.

6 Conclusion

In this work, we propose a new challenging task, OVCOS, to explore open-vocabulary semantic image segmentation (OVSIS) for the camouflaged objects in more complex natural scenes, and carefully collect and construct a large-scale data benchmark OVCamo. Meanwhile, by considering the characteristics of the task and data, we propose a strong single-stage baseline OVCoser with the advanced pre-trained vision-language model. Specifically, the well-designed prompt templates are introduced to reinforce the task-relevant semantic context. We introduce additional multi-source information including class semantic cues, depth spatial structure, object edge details, and top-down iterative guidance from the output space. With the help of these components, OVCoser can perceive and segment camouflaged objects in complex environments. Extensive experiments demonstrate the effectiveness of the proposed method and its superior performance compared with the existing state-of-the-art OVSIS algorithms on OVCamo.

References

- Anderson, P., He, X., Buehler, C., Teney, D., Johnson, M., Gould, S., Zhang, L.: Bottom-up and top-down attention for image captioning and visual question

- answering. In: Proceedings of IEEE Conference on Computer Vision and Pattern Recognition (2018) **9**
2. Bideau, P., Learned-Miller, E.: It's moving! a probabilistic model for causal motion segmentation in moving camera videos. In: Proceedings of European Conference on Computer Vision (2016) **5**
 3. Caesar, H., Bankiti, V., Lang, A.H., Vora, S., Liong, V.E., Xu, Q., Krishnan, A., Pan, Y., Baldan, G., Beijbom, O.: nuscenes: A multimodal dataset for autonomous driving. In: Proceedings of IEEE Conference on Computer Vision and Pattern Recognition (2020) **2**
 4. Caesar, H., Uijlings, J., Ferrari, V.: Coco-stuff: Thing and stuff classes in context. In: Proceedings of IEEE Conference on Computer Vision and Pattern Recognition (2018) **2, 6, 11**
 5. Chen, Y.C., Li, L., Yu, L., El Kholy, A., Ahmed, F., Gan, Z., Cheng, Y., Liu, J.: Uniter: Universal image-text representation learning. In: Proceedings of European Conference on Computer Vision (2020) **3**
 6. Cheng, B., Misra, I., Schwing, A.G., Kirillov, A., Girdhar, R.: Masked-attention mask transformer for universal image segmentation. Proceedings of IEEE Conference on Computer Vision and Pattern Recognition (2022) **2, 4**
 7. Cheng, B., Schwing, A., Kirillov, A.: Per-pixel classification is not all you need for semantic segmentation. International Conference on Neural Information Processing Systems (2021) **2, 4**
 8. Cheng, X., Xiong, H., Fan, D.P., Zhong, Y., Harandi, M., Drummond, T., Ge, Z.: Implicit motion handling for video camouflaged object detection. In: Proceedings of IEEE Conference on Computer Vision and Pattern Recognition (2022) **5, 11**
 9. Cherti, M., Beaumont, R., Wightman, R., Wortsman, M., Ilharco, G., Gordon, C., Schuhmann, C., Schmidt, L., Jitsev, J.: Reproducible scaling laws for contrastive language-image learning. Proceedings of IEEE Conference on Computer Vision and Pattern Recognition (2022) **2, 3, 7, 10**
 10. Cho, S., Shin, H., Hong, S., An, S., Lee, S., Arnab, A., Seo, P.H., Kim, S.W.: Cat-seg: Cost aggregation for open-vocabulary semantic segmentation. arXiv preprint (2023) **4, 10, 11, 14**
 11. Csurka, G., Volpi, R., Chidlovskii, B.: Semantic image segmentation: Two decades of research. Foundations and Trends in Computer Graphics and Vision (2022) **2**
 12. Everingham, M., Van Gool, L., Williams, C.K., Winn, J., Zisserman, A.: The pascal visual object classes (voc) challenge. International Journal of Computer Vision (2010) **2**
 13. Fan, D.P., Ji, G.P., Cheng, M.M., Shao, L.: Concealed object detection. IEEE Transactions on Pattern Analysis and Machine Intelligence (2021) **5, 11**
 14. Fan, D.P., Ji, G.P., Sun, G., Cheng, M.M., Shen, J., Shao, L.: Camouflaged object detection. In: Proceedings of IEEE Conference on Computer Vision and Pattern Recognition (2020) **5**
 15. Fan, D.P., Ji, G.P., Xu, P., Cheng, M.M., Sakaridis, C., Van Gool, L.: Advances in deep concealed scene understanding. Visual Intelligence (2023) **3, 5**
 16. Fan, D.P., Zhou, T., Ji, G.P., Zhou, Y., Chen, G., Fu, H., Shen, J., Shao, L.: Inf-net: Automatic covid-19 lung infection segmentation from ct images. IEEE Transactions on Medical Imaging (2020) **5**
 17. Ghiasi, G., Gu, X., Cui, Y., Lin, T.Y.: Scaling open-vocabulary image segmentation with image-level labels. In: Proceedings of European Conference on Computer Vision (2022) **10**

18. Gu, X., Lin, T.Y., Kuo, W., Cui, Y.: Open-vocabulary object detection via vision and language knowledge distillation. In: International Conference on Learning Representations (2021) [9](#), [10](#), [13](#)
19. He, K., Gkioxari, G., Dollar, P., Girshick, R.: Mask r-cnn. *IEEE Transactions on Pattern Analysis and Machine Intelligence* (Feb 2020) [2](#)
20. He, K., Zhang, X., Ren, S., Sun, J.: Deep residual learning for image recognition. In: Proceedings of IEEE Conference on Computer Vision and Pattern Recognition (2016) [10](#)
21. Jia, Q., Yao, S., Liu, Y., Fan, X., Liu, R., Luo, Z.: Segment, magnify and reiterate: Detecting camouflaged objects the hard way. In: Proceedings of IEEE Conference on Computer Vision and Pattern Recognition (2022) [5](#)
22. Katsuki, F., Constantinidis, C.: Bottom-up and top-down attention: different processes and overlapping neural systems. *The Neuroscientist* (2014) [9](#)
23. Le, T.N., Nguyen, T.V., Nie, Z., Tran, M.T., Sugimoto, A.: Anabranch network for camouflaged object segmentation. *Computer Vision and Image Understanding* (2019) [5](#)
24. Li, A., Zhang, J., Lyu, Y., Liu, B., Zhang, T., Dai, Y.: Uncertainty-aware joint salient object and camouflaged object detection. In: Proceedings of IEEE Conference on Computer Vision and Pattern Recognition (2021) [5](#)
25. Li, G., Duan, N., Fang, Y., Gong, M., Jiang, D.: Unicoder-vl: A universal encoder for vision and language by cross-modal pre-training. In: AAAI Conference on Artificial Intelligence (2020) [3](#)
26. Li, X., Yin, X., Li, C., Zhang, P., Hu, X., Zhang, L., Wang, L., Hu, H., Dong, L., Wei, F., et al.: Oscar: Object-semantics aligned pre-training for vision-language tasks. In: Proceedings of European Conference on Computer Vision (2020) [3](#)
27. Liang, F., Wu, B., Dai, X., Li, K., Zhao, Y., Zhang, H., Zhang, P., Vajda, P., Marculescu, D.: Open-vocabulary semantic segmentation with mask-adapted clip. *Proceedings of IEEE Conference on Computer Vision and Pattern Recognition* (2022) [4](#), [10](#), [11](#), [14](#)
28. Litjens, G., Kooi, T., Bejnordi, B.E., Setio, A.A.A., Ciompi, F., Ghafoorian, M., van der Laak, J.A., van Ginneken, B., Sánchez, C.I.: A survey on deep learning in medical image analysis. *Medical Image Analysis* (2017) [2](#)
29. Liu, L., Wang, R., Xie, C., Yang, P., Wang, F., Sudirman, S., Liu, W.: Pestnet: An end-to-end deep learning approach for large-scale multi-class pest detection and classification. *IEEE Access* (2019) [5](#)
30. Liu, Z., Lin, Y., Cao, Y., Hu, H., Wei, Y., Zhang, Z., Lin, S., Guo, B.: Swin transformer: Hierarchical vision transformer using shifted windows. *Proceedings of the IEEE International Conference on Computer Vision* (2021) [10](#)
31. Loshchilov, I., Hutter, F.: Decoupled weight decay regularization. In: International Conference on Learning Representations (2019) [10](#)
32. Lyu, Y., Zhang, J., Dai, Y., Li, A., Liu, B., Barnes, N., Fan, D.P.: Simultaneously localize, segment and rank the camouflaged objects. In: Proceedings of IEEE Conference on Computer Vision and Pattern Recognition (2021) [5](#)
33. Mithun, N.C., Panda, R., Papalexakis, E.E., Roy-Chowdhury, A.K.: Webly supervised joint embedding for cross-modal image-text retrieval. In: Proceedings of the ACM International Conference on Multimedia (2018) [3](#)
34. Mottaghi, R., Chen, X., Liu, X., Cho, N.G., Lee, S.W., Fidler, S., Urtasun, R., Yuille, A.: The role of context for object detection and semantic segmentation in the wild. In: Proceedings of IEEE Conference on Computer Vision and Pattern Recognition (2014) [2](#)

35. Neuhold, G., Ollmann, T., Bulo, S.R., Kotschieder, P.: The mapillary vistas dataset for semantic understanding of street scenes. In: Proceedings of the IEEE International Conference on Computer Vision (2017) [2](#)
36. Pang, Y., Zhao, X., Xiang, T.Z., Zhang, L., Lu, H.: Zoom in and out: A mixed-scale triplet network for camouflaged object detection. In: Proceedings of IEEE Conference on Computer Vision and Pattern Recognition (2022) [5](#)
37. Radford, A., Kim, J.W., Hallacy, C., Ramesh, A., Goh, G., Agarwal, S., Sastry, G., Askell, A., Mishkin, P., Clark, J., et al.: Learning transferable visual models from natural language supervision. In: Proceedings of the International Conference on Machine Learning (2021) [2](#), [3](#), [4](#), [7](#), [9](#), [10](#), [13](#), [14](#)
38. Ranftl, R., Bochkovskiy, A., Koltun, V.: Vision transformers for dense prediction. In: Proceedings of the IEEE International Conference on Computer Vision (2021) [10](#)
39. Rizzo, M., Marcuzzo, M., Zangari, A., Gasparetto, A., Albarelli, A.: Fruit ripeness classification: A survey (2023) [5](#)
40. Rombach, R., Blattmann, A., Lorenz, D., Esser, P., Ommer, B.: High-resolution image synthesis with latent diffusion models. In: Proceedings of IEEE Conference on Computer Vision and Pattern Recognition (2022) [10](#)
41. Skurowski, P., Abdulameer, H., Błaszczuk, J., Depta, T., Kornacki, A., Koziel, P.: Animal camouflage analysis: Chameleon database (2017), <http://kgwisc.aei.polsl.pl/index.php/pl/dataset/63-animal-camouflage-analysis> [5](#)
42. Su, W., Zhu, X., Cao, Y., Li, B., Lu, L., Wei, F., Dai, J.: Vi-bert: Pre-training of generic visual-linguistic representations. In: International Conference on Learning Representations (2019) [3](#)
43. Sun, Y., Wang, S., Chen, C., Xiang, T.Z.: Boundary-guided camouflaged object detection. In: International Joint Conference on Artificial Intelligence (2022) [8](#), [9](#)
44. Thisanke, H., Deshan, C., Chamith, K., Seneviratne, S., Vidanaarachchi, R., Herath, D.: Semantic segmentation using vision transformers: A survey. arXiv preprint (2023) [2](#)
45. Vaswani, A., Shazeer, N., Parmar, N., Uszkoreit, J., Jones, L., Gomez, A.N., Kaiser, u., Polosukhin, I.: Attention is all you need. In: International Conference on Neural Information Processing Systems (2017) [8](#), [9](#)
46. Xiang, M., Zhang, J., Lv, Y., Li, A., Zhong, Y., Dai, Y.: Exploring depth contribution for camouflaged object detection (2022) [8](#)
47. Xu, J., Liu, S., Vahdat, A., Byeon, W., Wang, X., De Mello, S.: Open-vocabulary panoptic segmentation with text-to-image diffusion models. In: Proceedings of IEEE Conference on Computer Vision and Pattern Recognition (2023) [4](#), [10](#), [11](#), [14](#)
48. Xu, M., Zhang, Z., Wei, F., Hu, H., Bai, X.: Side adapter network for open-vocabulary semantic segmentation. Proceedings of IEEE Conference on Computer Vision and Pattern Recognition (2023) [2](#), [4](#), [10](#), [11](#), [14](#)
49. Xu, M., Zhang, Z., Wei, F., Lin, Y., Cao, Y., Hu, H., Bai, X.: A simple baseline for open-vocabulary semantic segmentation with pre-trained vision-language model. In: Proceedings of European Conference on Computer Vision (2021) [4](#), [10](#), [11](#), [14](#)
50. Yang, J.: Plantcamo dataset (2023), <https://github.com/yjybuua/PlantCamo> [5](#)
51. Yin, B., Zhang, X., Hou, Q., Sun, B.Y., Fan, D.P., Van Gool, L.: Camoformer: Masked separable attention for camouflaged object detection (2022) [5](#), [9](#)
52. Yu, Q., He, J., Deng, X., Shen, X., Chen, L.C.: Convolutions die hard: Open-vocabulary segmentation with single frozen convolutional clip. In: International Conference on Neural Information Processing Systems (2023) [4](#), [10](#), [11](#), [14](#)

53. Zabari, N., Hoshen, Y.: Open-vocabulary semantic segmentation using test-time distillation. In: European Conference on Computer Vision Workshops (2023) [4](#)
54. Zhang, W., Pang, J., Chen, K., Loy, C.C.: K-net: Towards unified image segmentation. International Conference on Neural Information Processing Systems (2021) [2](#)
55. Zhao, H., Puig, X., Zhou, B., Fidler, S., Torralba, A.: Open vocabulary scene parsing. In: Proceedings of the IEEE International Conference on Computer Vision (2017) [4](#)
56. Zheng, Y., Zhang, X., Wang, F., Cao, T., Sun, M., Wang, X.: Detection of people with camouflage pattern via dense deconvolution network. IEEE Signal Processing Letters (Jan 2019) [5](#)
57. Zhou, B., Zhao, H., Puig, X., Fidler, S., Barriuso, A., Torralba, A.: Scene parsing through ade20k dataset. In: Proceedings of IEEE Conference on Computer Vision and Pattern Recognition (2017) [2](#), [6](#)
58. Zhou, C., Loy, C.C., Dai, B.: Extract free dense labels from clip. In: Proceedings of European Conference on Computer Vision (2022) [4](#)
59. Zhou, H., Shen, T., Yang, X., Huang, H., Li, X., Qi, L., Yang, M.H.: Rethinking evaluation metrics of open-vocabulary segmentaion. ArXiv [abs/2311.03352](#) (2023) [6](#)
60. Zhou, K., Yang, J., Loy, C.C., Liu, Z.: Learning to prompt for vision-language models. International Journal of Computer Vision (2021) [9](#), [10](#)
61. Zhu, C., Chen, L.: A survey on open-vocabulary detection and segmentation: Past, present, and future. arXiv preprint (2023) [2](#), [4](#), [11](#)
62. Zhu, F., Zhu, Y., Lee, V., Liang, X., Chang, X.: Deep learning for embodied vision navigation: A survey. arXiv preprint (2021) [2](#)